International Journal of Nanomedicine

Dovepress
Taylor & Francis Group

Open Access Full Text Article

ORIGINAL RESEARCH

Synergistic Effect of Doxorubicin-Thermo-Iodized Oil Pickering Emulsions on the Interventional Embolization-Chemotherapy- Immunity of VX2 Rabbit Liver Cancer

Ling Li[1,2,*], Wenjing Xie[3,4,*], Haixia Sun[5,*], Houqiang Yu[1], Cai Wang[1], Min Zheng[1], Peng Shi[5], Hongan Tian[2], Tongqiang Xiong[1,4]

[1]School of Biomedical Engineering and Imaging, Xianning Medical College, Hubei University of Science and Technology, Xianning, People's Republic of China; [2]Department of Radiology, Xianning Central Hospital, The First Affiliated Hospital of Hubei University of Science and Technology, Xianning, People's Republic of China; [3]Guang'an Traditional Chinese Medicine Hospital, Guang'an, People's Republic of China; [4]School of Automation, Hubei University of Science and Technology, Xianning, 437100, People's Republic of China; [5]School of Biomedical Sciences and Engineering, Guangzhou International Campus, South China University of Technology, Guangzhou, People's Republic of China

*These authors contributed equally to this work

Correspondence: Hongan Tian, Department of Radiology, Xianning Central Hospital, The First Affiliated Hospital of Hubei University of Science and Technology, Xianning, 437100, People's Republic of China, Email tihongan@163.com; Tongqiang Xiong, School of Biomedical Engineering and Imaging, Xianning Medical College, Hubei University of Science and Technology, Xianning, 437100, People's Republic of China, Email Xiongtongqiang@hbust.edu.cn

Background: Tumor recurrence and metastasis are important factors affecting the efficacy of transhepatic arterial chemoembolization. To prolong the survival of patients, comprehensive interventional therapy and antitumor drugs that can control their release need to be developed.

Methods: Poly(N-isopropylacrylamide-co-acrylic acid) nanogels are firstly self-assembled with doxorubicin, the constructed doxorubicin-loaded nanogels were then emulsified with iodized oil under high-shear conditions to form doxorubicin–iodized oil nanogel suspensions (Dox-TIPE). The structural characteristics, thermosensitive properties and rheological properties were evaluated. The in vitro biocompatibility and drug release behavior of Dox-TIPE were assayed and in vivo interventional therapy was examined in a VX2 rabbit liver cancer model.

Results: Dox-TIPE can effectively exert the dual advantages of chemoembolization therapy, achieving a superior therapeutic effect on inhibiting rabbit liver tumor growth. It promotes TUNEL expression in the tumor boundary region while reducing Ki67 expression, which results in decreased tumor cell proliferation and increased apoptosis rates. Furthermore, Dox-TIPE effectively suppresses the expressions of HIF-1α, VEGF, and CD31 in tumor target areas, thereby preventing the formation of tumor neovascularization and collateral circulation.

Conclusion: We successfully produced Dox-TIPE which offers a multifunctional platform combining embolization, chemotherapy, imaging, and immunomodulation. This novel embolic material shows strong potential to address current limitations of TACE in liver cancer treatment and may serve as a promising candidate for next-generation embolization therapies.

Keywords: transcatheter arterial embolization, doxorubicin-loaded pickering emulsion, liver cancer, sustained release

Introduction

Hepatocellular carcinoma (HCC) is a highly malignant solid tumor and is often referred to as the "king of cancers" owing to its aggressiveness and poor prognosis. Although novel pharmacological agents and therapeutic strategies have advanced, the incidence and mortality rates of HCC are quite high.[1–3] With the rapid development of interventional radiology, transcatheter arterial chemoembolization (TACE) has emerged as one of the most widely used non-surgical treatments for patients with intermediate-to-advanced-stage HCC.[4–6] By delivering embolic agents into the arterial

https://doi.org/10.2147/IJN.S569851
Received: 3 November 2025
Accepted: 19 May 2026
Published: 25 May 2026

Graphical Abstract

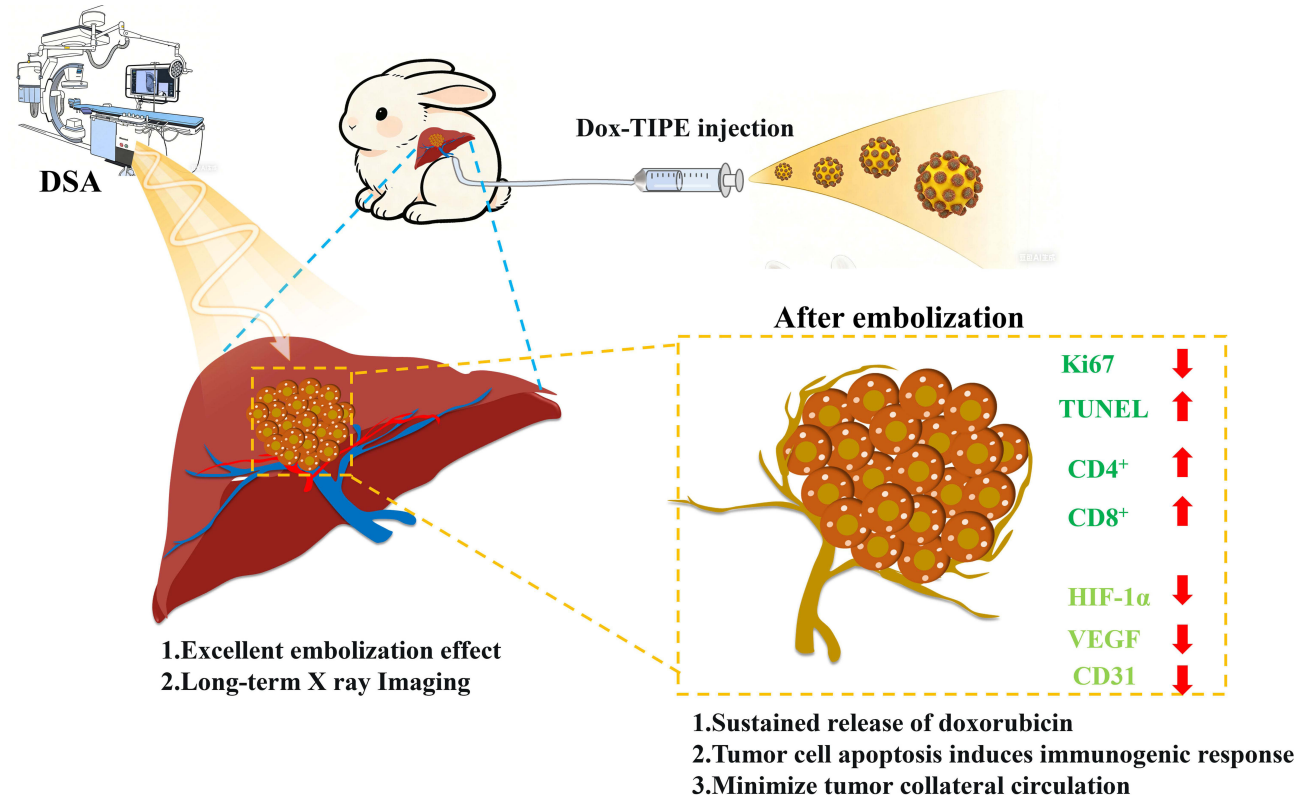

supply of the tumor, TACE achieves dual therapeutic effects: localized delivery of chemotherapeutic agents and arterial occlusion to induce ischemic tumor necrosis.[7,8] The efficacy of TACE highly depends on the physicochemical properties and biological performance of the embolic agents used. Conventional embolic materials are generally classified as either solid or liquid. Solid embolic agents, such as drug-eluting beads or microspheres, offer durable occlusion and mechanical stability but are limited by their particle size, which restricts their penetration into the tumor microvasculature and may facilitate the development of collateral circulation.[9,10] Liquid embolic agents such as Lipiodol exhibit high fluidity and distal penetration, allowing deeper infiltration into tumor-feeding capillaries. However, their embolic strength and retention are suboptimal, often requiring combination therapy with solid embolic agents to achieve satisfactory outcomes.

Generally, TACE procedures are performed under real-time fluoroscopic guidance via digital subtraction angiography (DSA), which requires embolic agents with adequate radiopacity. Most commercially available solid embolic agents lack intrinsic radiopacity and must be mixed with external contrast agents, which may result in inconsistent imaging, short-term visibility, and inaccurate assessment of embolization endpoints. Transcatheter arterial chemoembolization (TACE) serves not only as a localized embolization procedure but also as an efficient drug delivery platform. By incorporating therapeutic agents into embolic agents, sustained drug release can be achieved, thereby increasing local efficacy while decreasing systemic toxicity.[9,10] Therefore, an ideal embolic material for TACE must have the following attributes: excellent injectability and fluidity, strong and sustained embolization capability, intrinsic radiopacity for imaging, and effective drug loading and controlled release performance. Iodized oil-based emulsions mixed with chemotherapeutic agents are widely used in clinical TACE practice.[11,12] However, these systems have several drawbacks, including poor emulsion stability, rapid phase separation, short retention time in the vasculature, and suboptimal drug release profiles. Some studies have reported that the long-term clinical outcome of TACE is closely related to the physical and biological characteristics of the embolic agents used.[13–15]

Pickering emulsions, a novel type of emulsion system stabilized by solid particles instead of traditional surfactants, have gained considerable attention in recent years.[16–18] Nanoparticle-stabilized Pickering emulsions have high biocompatibility, structural stability, and environmental safety. They are highly promising in pharmaceutical applications, particularly in improving the stability of emulsions, increasing the bioavailability of poorly soluble drugs, and enabling sustained release.[19–21] As described in previous studies,[22–25] we developed a thermosensitive iodized oil Pickering emulsion (TIPE) with a high oil-to-water ratio, using nanogels to encapsulate and stabilize iodized oil. This formulation overcomes the limitations of conventional iodized oil emulsions, including phase instability and weak embolic strength. In rabbit renal artery embolization experiments, TIPE achieved effective and durable vascular occlusion, resulting in extensive ischemic necrosis and calcification, and showed excellent embolic and radiographic properties.

Based on these findings, we developed a novel oil-in-water (O/W) Pickering emulsion hydrogel composite known as Dox-TIPE, which integrates thermosensitivity, radiopacity, and drug delivery functionality. In the VX2 orthotopic rabbit liver tumor model, Dox-TIPE undergoes a temperature-triggered sol-gel transition, resulting in sustained hepatic arterial embolization and complete interruption of the tumor blood supply. This formulation significantly improved the tumor immune microenvironment, induced tumor cell necrosis and apoptosis, and facilitated the sustained release of doxorubicin, resulting in a synergistic chemoembolization effect. Moreover, the O/W emulsion structure effectively retained iodized oil, enhanced imaging contrast in the embolized region, and facilitated postoperative CT follow-up after TACE (Scheme 1).

Materials and Methods

Materials

N-Isopropylacrylamide (NIPAM) and acrylic acid (AA) were purchased from Tokyo Co., Ltd., Japan. Octadecyltrimethylammonium chloride (STAC), 2,2'-azobis(2-methylpropane amidine) dihydrochloride (AAPH), and rhodamine-B were purchased from Aladdin Chemical Reagent Co., Ltd.; 4% paraformaldehyde was purchased from McLean Reagent Co., Ltd.; iodixanol (I, 300 mg/mL) was purchased from Jiangsu Hengrui Medicine Co., Ltd; iodized oil (480 mg I/mL) was purchased from Jiangsu Hengrui Medicine Co., Ltd.; polyvinyl alcohol particle embolic agents (710 μm–1100 μm) were purchased from Hangzhou Ailikang Pharmaceutical Technology Co., Ltd.; lidocaine hydrochloride, gentamicin sulfate, and penicillin sodium were purchased from North China Pharmaceutical Co., Ltd.; medical iodophor disinfectant was purchased from Shandong Lierkang Medical Technology Co., Ltd.; heparin sodium injection was purchased from Changzhou Qianhong Biochemical Pharmaceutical Co., Ltd.; 0.9% sodium chloride injection was purchased from Wuhan Binhu Double Crane Pharmaceutical Co., Ltd. Vascular puncture set, 18G puncture needle, 4F vascular sheath, short guide wire, 4 F Cobra catheter, and 0.035' hydrophilic super-smooth guide wire were all purchased from Terumo, Japan. Surgical instruments and a femoral arteriotomy kit were purchased from Zibo Chuangqi Medical Supplies Co., Ltd. Milli-Q ultrapure water (18.2 MΩ) was used in all experiments.

Preparation and Characterization of Dox-Poly (N-Isopropylacrylamide- Co-Acrylic Acid) (Dox-PNCAA)

We prepared PNCAA following the methods described in other studies.[24,25] Dox was dissolved in a PNCAA aqueous dispersion (details in Table S1) to prepare Dox-PNCAA (details in Supporting Information 1. Preparation of Doxorubicin-Loaded PNCAA Nanogels). The average particle sizes of PNCAA and Dox-PNCAA were determined by dynamic light scattering (DLS, Zetasizer Nano ZS90, Malvern Instrument Ltd., UK) with a 4 mW He-Ne laser source (λ= 633 nm) and a scattering angle of 90°. All samples were diluted with ultrapure water to 0.1 wt%. The microscopic morphologies of PNCAA and Dox-PNCAA were characterized by TEM at 200 kV (Tecnai G2 20 FEI Corp., Netherlands). Thermogravimetric analysis (EXSTAR TG/DTA 6000 Series, SII NanoTechnology Inc., Tokyo, Japan) was performed to evaluate the changes in the weights of PNCAA and Dox-PNCAA freeze-dried powders as the temperature increased over time.

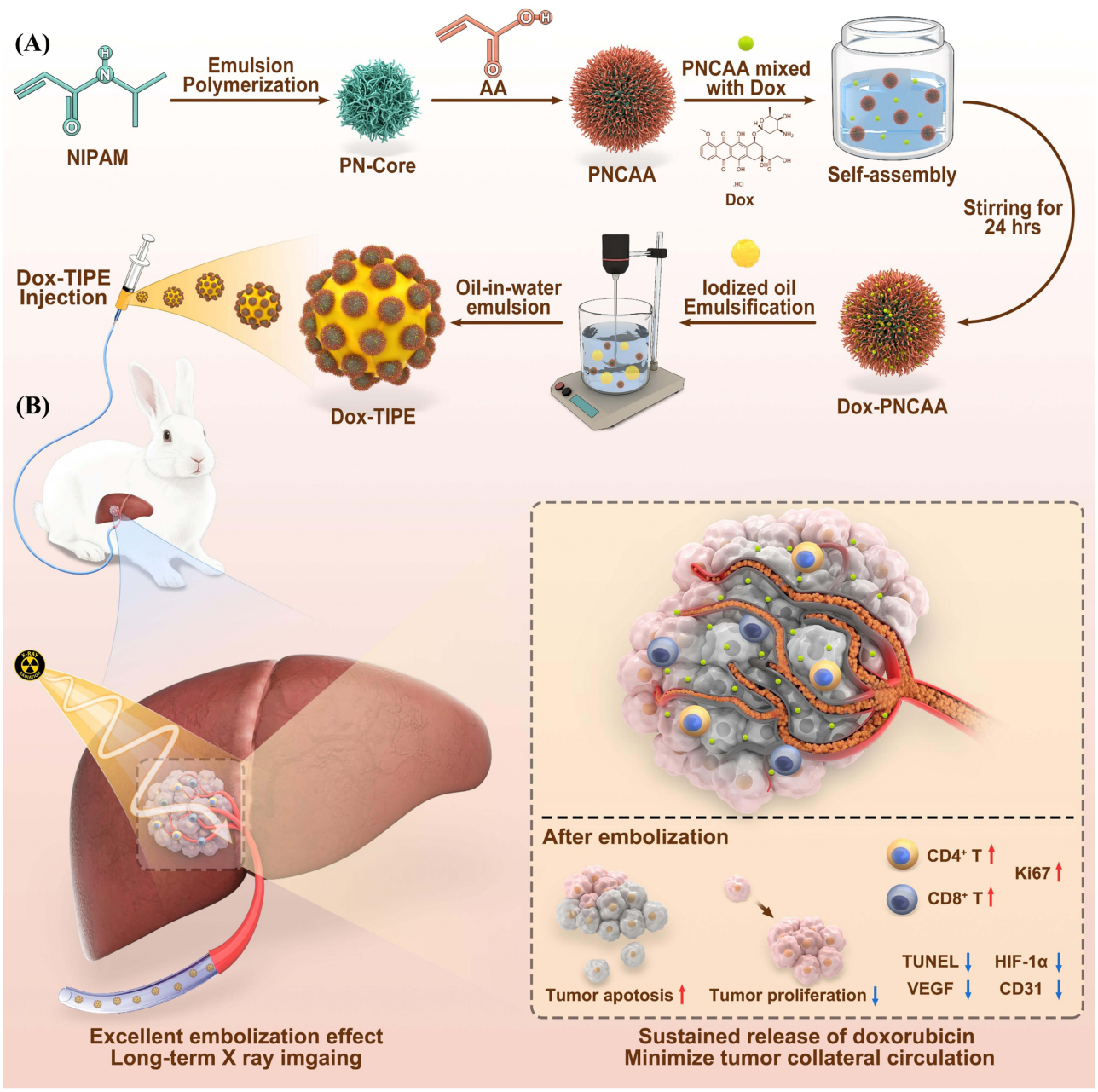

Scheme 1 Schematic representation of the synergistic effect of a doxorubicin-thermo-iodized oil Pickering emulsion on the interventional embolization-chemotherapy-immunity of VX2 rabbit liver cancer. (**A**) Preparation of Pickering emulsions loaded with doxorubicin. (**B**) Study of the effects of Pickering emulsions loaded with doxorubicin on the chemoembolization synergy and immune microenvironment of VX2 rabbit liver tumors. Red arrows indicate an increase, whereas blue arrows indicate a decrease.

Preparation and Characterization of a Dox-Thermosensitive Iodized Oil Pickering Emulsion (Dox-TIPE)

Dox-PNCAA was emulsified with iodized oil via high-speed shearing to formulate Dox-TIPE, with water/oil (W/O) ratios of 8:2, 7:3, and 6:4 (Table S2). The stability of the emulsions and the extent of phase separation were evaluated at room temperature. The optimal W/O ratio was determined based on the visual assessment of the stability of the emulsions and the degree of water-oil separation.

The rheological properties of the samples were analyzed using a rotational rheometer. A parallel plate geometry with a 0.5 mm gap was used. Under a constant shear stress of 0.5 Pa, the storage modulus (G') and loss modulus (G') were recorded as a function of temperature from 25 °C to 45 °C at a heating rate of 2.0 °C/min and a fixed frequency of 1.0 Hz

to evaluate the thermoresponsive behavior. Additionally, to investigate the shear-thinning properties, the viscosity of the samples was measured at 25 °C under various shear rates ranging from $50s^{-1}$ to 2800 s^{-1}.

For the in vitro injectability assessment, a 6 wt% 20Dox-TIPE (containing 20mg of doxorubicin) hydrogel was preloaded into a 1 mL syringe and a 5 mL syringe equipped with a plastic catheter. The formulation was injected into water maintained at 37 °C at a consistent rate to simulate clinical administration, and its extrusion behavior under physiological conditions was evaluated.

To study the drug release profile, 2 mL of each hydrogel formulation (6 wt% 10Dox-TIPE, 20Dox-TIPE, and 30Dox-TIPE) was allowed to undergo sol-gel transition at 37 °C and then immersed in release media (pH 5.0, 6.8, and 7.4, respectively). The samples were placed in a thermostatic shaker at 37 °C and agitated at a constant speed. At predetermined time points (1 h, 3 h, 6 h, 12 h, 24 h, 48 h, 72 h, 96 h, and 120 h), 3 mL of the release medium was collected for analysis and immediately replenished with 3 mL of fresh medium of the same pH. The collected samples were analyzed using a UV-Vis spectrophotometer (Beijing General Analytical Instrument Co., Ltd., Beijing, China) at 480 nm. The cumulative release of doxorubicin was calculated based on the absorbance values and a standard calibration curve.

Assessing Vascular Embolization Capacity in Ex Vivo Organs via Decellularization (details in Supporting Information 2. Preparation of decellularized liver).

Evaluation of Dox-TIPE for TACE in a VX2 Rabbit Liver Tumor Model

Rabbit VX2 Liver Tumor Model

All animal studies were conducted following the Guidelines for the Care and Use of Laboratory Animals established by the Science and Technology Department of Hubei Province, China. The study was approved by the Animal Ethics Committee of Hubei University of Science and Technology, China (Approval No.: 2024–02-002). Adult New England white rabbits (weighing 2.5–3.0 kg, hermaphrodite) were purchased from the Laboratory Animal Center of Hubei University of Science and Technology (Xianning, China). All animals were housed under controlled conditions: 16–28 °C, 8–10 air exchanges/day, illumination 150–300 lx, noise ≤60 dB, and free access to food and water.

A VX2 tumor-bearing Japanese big-eared rabbit was anesthetized with 2.0 wt.% sodium pentobarbital (30 mg/kg). After disinfection, viable tumor tissue was excised, rinsed with PBS, cut into ~1 mm^3 fragments, and stored in Hanks' solution. Next, rabbits (n = 16; weight: 2.5–3.0 kg) were starved for 12 h and anesthetized. A midline abdominal incision was made to expose the liver. A small incision (~1 cm) was made in the left outer lobe, and a VX2 tumor fragment was implanted and secured with a gelatin sponge. After hemostasis, the liver was repositioned. Gentamicin was applied locally, and ampicillin was administered intramuscularly for three days. The tumors were allowed to grow for 17 days. When the tumor reached ~1.61×10^3 mm^3, TACE was performed. After confirming that the tumors were implanted, 16 experimental rabbits were randomly assigned to three groups (n = 3 rabbits per group): normal saline (NS), doxorubicin-iodized oil (Dox-IO), and Dox-TIPE.

TACE Procedure

After abstaining from eating and drinking for 12 h, the rabbits were anesthetized by injecting 30 mg/kg pentobarbital sodium through their auricular veins and fixed in the supine position after pain sensation has diminished in 5–10 min. Next, 1 mL of 4% lidocaine was subcutaneously injected. A small incision was made in the groin, and blunt dissection was performed to expose the femoral artery. The distal end was ligated, and a vascular clamp was applied to the proximal end. A puncture needle was used to access the artery, and when blood return was detected, a short guidewire was inserted. The needle cannula was withdrawn, and a 4F vascular sheath was introduced and secured with sutures. Next, heparinized saline (1:500, v/v) was flushed through the sheath, and catheterization was confirmed.

The rabbits were then transferred to the angiography suite for DSA. A 4F Cobra catheter was advanced via the sheath into the celiac artery under guidewire guidance. After the guidewire was removed, a contrast mixture of iodixanol (350 mg I/mL) and heparinized saline was injected to confirm arterial access. The catheter was flushed with deionized water and connected to a high-pressure injector. Celiac arteriography was performed at a flow rate of 1 mL/s (total volume: 3 mL; pressure: 200 kPa).

A microcatheter was used to superselect the tumor-feeding artery, and its tip was positioned within the tumor vasculature. Embolic agents were administered at a flow rate of 0.5 mL/s (total volume: 0.5 mL; pressure: 200 kPa). Each animal group received the following doses via intra-arterial injection: NS (0.3 mL), Dox-IO (0.3 mL), or Dox-TIPE (0.3 mL).

Imaging Evaluation Methods

Contrast-enhanced CT scans were performed on days 0, 7, and 14 post-TACE to monitor tumor progression. Each rabbit received a 3 mL intravenous injection of iodixanol via the marginal ear vein. The scanning parameters were as follows: tube voltage, 80 kV; tube current, 60 mA; initial positioning; and arterial (15 s), venous (25 s), and delayed (45 s) phases. The hepatic artery, its branches, and the peripheral vasculature were evaluated to assess the efficacy of embolization.

The tumor dimensions (left-right, anterior-posterior, and superior-inferior) were measured in the enhanced CT images across all three phases to calculate the tumor volume and growth rate. The tumor volume (V) was calculated using the ellipsoid formula:

$$V\left(cm^3\right) = \frac{a \times b \times c \times \pi}{6}$$

Here, a, b, and c represent the maximum tumor diameters in the left-right, anterior-posterior, and superior-inferior directions, respectively.

The tumor growth rate (%) was calculated as follows:

$$\text{Tumor growth rate}(\%) = \frac{Vt}{V0} \times 100\%$$

Here, V_0 represents the tumor volume on day 0 (pretreatment) and V_t represents the tumor volume on day t after TACE.

Assessment of Dox Distribution in Tumors

Excessive 2.0 wt.% sodium pentobarbital is injected into the marginal ear vein of experimental rabbits to implement humanitarian euthanasia on days 1 and 3 after TACE. Liver tumor tissues were harvested, immediately frozen at −80 °C, and sectioned into ~4 μm slices using a cryostat. The distribution and release behavior of doxorubicin were assessed using an Olympus fluorescence microscope (excitation: 475–485 nm; emission: 575–585 nm; green channel).

Frozen sections of tumors treated with iodized oil-based Pickering gel emulsions were imaged at 50× magnification. The fluorescence intensity was quantified in four randomly selected regions per section using the Image-Pro Plus 6.0 software. The average fluorescence intensity was used to evaluate the intratumoral release profile of doxorubicin one, three, and 14 days after embolization.

Impact of Dox-TIPE-Based TACE on the Tumor Immune Microenvironment

All experimental rabbits were injected with an excessive dose of 2.0 wt.% sodium pentobarbital into the marginal ear vein to implement humanitarian euthanasia on 14 days after TACE treatment. Death was confirmed by the absence of spontaneous breathing and corneal reflexes. Subsequently, the liver tumors, hearts, spleens, lungs, and kidneys were harvested and photographed. The collected tissues were fixed in 4% paraformaldehyde, embedded in paraffin, and sectioned. The slides were deparaffinized with xylene and rehydrated through a graded ethanol series for hematoxylin and eosin (H&E) staining. Histological examinations were performed under a light microscope.

The necrotic area of each liver tumor was quantified by analyzing H&E-stained sections, and the tumor necrosis rate (TNR) was calculated using the following formula:

$$TNR = \frac{n}{n + t} \times 100$$

Here, n indicates the necrotic area, and *t* indicates the area of viable tumor tissue.

Apoptotic cells were detected by conducting the terminal deoxynucleotidyl transferase dUTP nick end labeling (TUNEL) assay. The sections were incubated with proteinase K (20 μg/mL) at 37 °C for 20 min, rinsed, and incubated in a TUNEL reaction mixture (1:9) at 37 °C for 1 h in the dark. After counterstaining with DAPI for 5 min, fluorescence was detected using a confocal microscope. TUNEL and Ki67 signals were captured at excitation/emission wavelengths

of 488/560 nm. The mean fluorescence intensity in four randomly selected fields (magnification: 200×) was quantified using Image-Pro Plus 6.0. The percentage of apoptotic or proliferating cells was calculated as the ratio of marker-positive cells to total nuclei.[26,27]

To conduct immunofluorescence assays, the slides were immersed in citrate buffer (0.01 mol/L, pH 6.0) and heated three times in a microwave (5 min each). Endogenous peroxidase activity was blocked with 3% H_2O_2 in methanol for 10 min. The sections were incubated overnight at 4 °C with the following primary antibodies: mouse anti-Ki67 (1:150), anti-HIF-1α (1:100), anti-VEGF (1:150), and anti-CD31 (1:50), anti-GULT1 (1:50), anti-CD3 (1:100), anti-CD4 (1:100), and anti-CD8 (1:100). After washing, the sections were incubated for 50 min at 37 °C with goat anti-rabbit secondary antibodies (1:150) and fluorescent-labeled antibodies (eg., FITC and Cy3), followed by nuclear staining with DAPI.

The following fluorescence signals were detected via confocal microscopy: Cy3 (Ex/Em = 554/650 nm), FITC (Ex/Em = 488/525 nm), and DAPI (Ex/Em = 350/460 nm).

The ImageJ software was used to quantify the integrated optical density (IOD) of four representative fields (200×). The percentage of positively stained area was calculated as follows:

$$\text{The percentage of areas with positive staining} = \frac{\%\text{mean of positive area}}{\text{Mean total ROI in samples}}$$

Biocompatibility Evaluation

HepG2 cells were maintained in our laboratory. The cytotoxic effects of iodized oil, TIPE, Dox, and Dox-TIPE on HepG2 cells were evaluated by conducting the MTT assay. HepG2 cells were seeded in 96-well plates at a density of 8×10^4 cells/well in DMEM and incubated overnight at 37 °C. Then, the medium was replaced with different concentrations of test samples diluted in DMEM and incubated for 24 h. DMEM without any treatment served as the negative control, and DMEM without cells was used as the blank control.

To investigate the cytotoxic mechanism, HepG2 cells treated with Dox-TIPE, DOX, TIPE, or saline were subjected to Annexin V-FITC/PI staining and flow cytometric analysis. (details in Supporting Information 3. Flow Cytometric Analysis of Cell Death and Apoptosis Staging in HEPG2 Cells Cell Culture and Treatment).

Statistical Analysis

All experimental data were expressed as the mean (x) ±standard deviation (SD), and the data were statistically analyzed using the IBM SPSS 21.0 statistical software. One-way analysis of variance (ANOVA) was conducted to compare the overall mean values of each group. Using the Bonferroni method, the difference was considered to be statistically significant at $P < 0.05$, and the charts were drawn using GraphPad Prism 9.0.

Results and Discussion

Structure and Morphology of Doxorubicin-Loaded Poly(N-Isopropylacrylamide -Co -Acrylic Acid) Gel

UV spectrophotometry (Figure 1A) revealed that Dox-PNCAA exhibited a red-shifted absorption peak around 490 nm, corresponding to the characteristic peak of doxorubicin, confirming its successful incorporation. TGA (Figure 1B) showed that Dox-PNCAA underwent greater weight loss compared to PNCAA, with a significant loss (~93.86 wt%) observed at ~117°C and further reaching 95.92 wt% above 128°C, indicating altered thermal degradation behavior upon DOX loading. Transmission electron microscopy (TEM) analysis demonstrated that the blank poly (N-isopropylacrylamide-*co*-acrylic acid) (PNCAA) exhibited a uniform spherical morphology with smooth surfaces and an average diameter of approximately 200 nm. Upon doxorubicin (Dox) encapsulation, the resulting Dox-PNCAA maintained their spherical architecture but developed a conspicuous electron-dense outer shell, indicative of successful drug loading. The pronounced peripheral contrast observed in these nanoparticles suggests the formation of a drug-rich bilayer configuration, which is anticipated to enhance nanocarrier stability and facilitate controlled drug release within tumor tissues (Figure 1C). The particle size of Dox-PNCAA showed a concentration-dependent increase with the

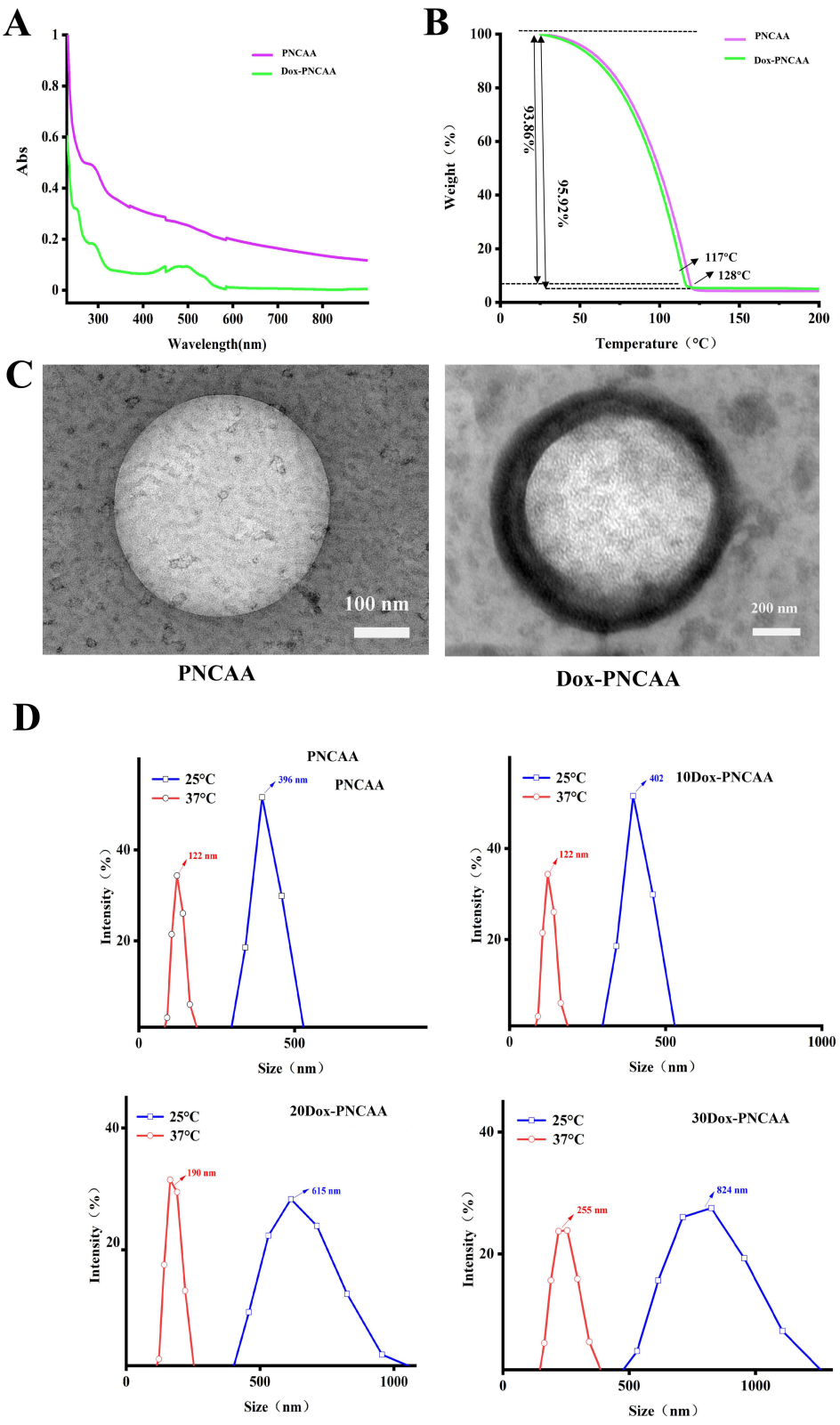

Figure 1 The fundamental characterization of PNCAA and Dox-PNCAA. (**A**) UV spectra of PNCAA and Dox-PNCAA. (**B**) TGA of PNCAA and Dox-PNCAA. (**C**) TEM image of PNCAA (left) and Dox-PNCAA (right). (**D**) Average particle size distribution of PNCAA and Dox-PNCAA.

https://doi.org/10.2147/IJN.S569851

addition of doxorubicin. At 25°C, the size increased from 396 nm to 824 nm, while at 37°C, it further increased from 122 nm to 255 nm. These findings suggest that doxorubicin may facilitate or induce the self-assembly of PNCAA (Figure 1D). PNCAA contains abundant carboxyl groups, which are negatively charged under physiological conditions, whereas DOX carries positive charges under the same conditions. Therefore, electrostatic interactions between PNCAA and DOX may lead to molecular aggregation, thereby inducing self-assembly behavior, as reflected by the significant increase in particle size. In addition, DOX contains aromatic ring structures that may interact with the hydrophobic microdomains of PNCAA through hydrophobic interactions and/orπ-πstacking at body temperature, further stabilizing the self-assembled structures.

Evaluation of Thermosensitivity of Dox-PNACAA and in Vitro Drug Release Study of Dox-TIPE

The transition temperature of Dox-PNCAA remained largely unchanged with increasing DOX content, indicating that drug loading did not significantly disrupt the balance between hydrophilic and hydrophobic interactions within the gel matrix. This was further supported by DSC analysis, which showed only a slight shift in the enthalpy peak position (Figure 2A).

The injectability and embolic performance of the nanogels were also evaluated by the vial inversion method (Figure 2B, Figure S1–S2, Video S1 and Video S2). To simulate in vivo embolization, Dox-PNCAA was injected at 37°C through a 2 mm catheter and a 1 mL syringe (needle diameter ~0.6 mm). The gel formed strips consistent with the lumen diameter, effectively occluding the vessel mimics and minimizing the risk of recanalization (Figure 2C).

The rheological properties of 20Dox-TIPE were assessed using a high-speed rotational rheometer to evaluate its injectability and embolization strength, thereby supporting smooth delivery during in vivo TACE procedures. As shown in Figure 2D, the embolization strength of 20Dox-TIPE reached approximately 1000 Pa, sufficient to occlude target vessels. With increasing shear rate, 20Dox-TIPE exhibited a clear shear-thinning behavior (Figure 2E). At 37 °C, under a pressure of 70 Pa, the resistance can still reach 10,000 Pa·s, which shows that 20Dox-TIPE has a certain hardness and embolism strength at 37 °C (Figure 2F).

The sustained release behavior of Dox-TIPE was further investigated under conditions mimicking the tumor microenvironment. Samples of 10Dox-TIPE, 20Dox-TIPE, and 30Dox-TIPE were incubated in release media at pH 5.0, 6.8, and 7.4. Doxorubicin concentrations were calculated based on UV absorbance and used to determine cumulative release profiles. As shown in Figures 2G–I, all formulations demonstrated pH-responsive release, with higher cumulative release observed under acidic conditions. Notably, 10Dox-TIPE released over 50% of DOX within 12 hours (Figure 2G), while 20Dox-TIPE and 30Dox-TIPE released approximately 40% and 25%, respectively (Figures 2H and I). Given the slightly acidic nature of the tumor microenvironment (pH ~6.8),[28,29] the sustained release behavior of 20Dox-TIPE is considered optimal for achieving effective and prolonged therapeutic outcomes. The experimental results demonstrate that DOX is released more rapidly and more completely under acidic conditions. This behavior can be mainly attributed to the protonation of acrylic acid (AA) units in PNCAA as the pH decreases, which leads to the gradual dissociation of the self-assembled structures originally formed through electrostatic interactions with DOX. As a result, the confinement of DOX within the system is weakened, thereby promoting drug release. In addition, the increased solubility of DOX under acidic conditions also contributes to its enhanced release at low pH.

Evaluation of Postoperative Imaging and Long-Term Embolization Effects of Dox-TIPE

To evaluate the postoperative imaging and long-term embolization efficacy of Dox-TIPE, VX2 tumor-bearing rabbits were randomly divided into three groups: Normal Saline, Dox-Iodized Oil, and Dox-TIPE (n = 4 per group). As shown in Figure 3A, the tumor regions were clearly visualized by pre-embolization imaging, and both Dox-Iodized Oil and Dox-TIPE achieved effective embolization, with follow-up imaging confirming complete blockage of tumor-associated vessels. Post-embolization angiography showed a clear loss of tumor perfusion and redistribution of contrast signals, indicating that both materials effectively occluded tumor-feeding arteries, including distal branches (Figure 3B).

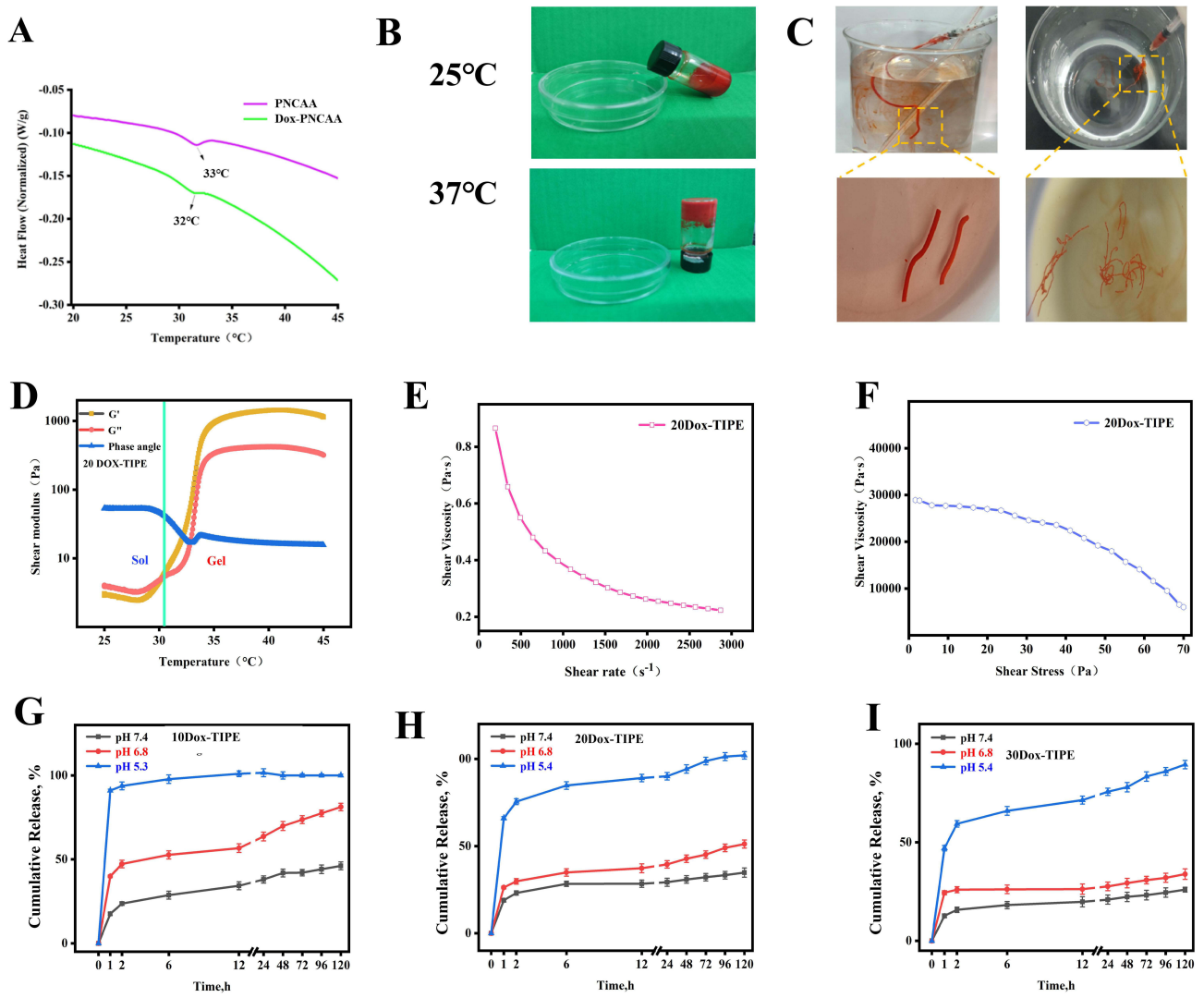

Figure 2 Evaluation of thermosensitivity of Dox-PNCAA. (**A**) The results of DSC and (**B**) Phase transition behavior of the Dox-TIPE at 25 and 37 °C. (**C**) Evaluation of the effect of in vitro simulated vascular casting. (**D**) 20Dox-TIPE viscoelastic analysis (**E**) 20Dox-TIPE shear thinning results. The green vertical line indicates the sol-gel transition temperature defined as the temperature at which G' and G" intersect, marking the point where the material transitions from a predominantly viscous, solution-like state (Sol, left of the green line) to a predominantly elastic, gel-like state (Gel, right of the green line). (**F**) 20Dox-TIPE anti-yield stress results. (**G**) Cumulative drug release rate of 10Dox-TIPE at pH 7.4, pH 6.8, pH 5.3 (**H**) Cumulative drug release rate of 20Dox-TIPE at pH 7.4, pH 6.8, pH 5.3. (**I**) Cumulative drug release rate of 30Dox-TIPE at pH 7.4, pH 6.8, pH 5.3.

To assess long-term vascular retention and imaging visibility, CT scans were performed on days 0, 7, and 14 post-treatment. Dox-TIPE exhibited superior long-term CT imaging capabilities compared to the conventional Dox-Iodized Oil formulation, as demonstrated by cross-sectional, sagittal, and 3D reconstructed images (Figure 3C; Figure S3–S5).

Tumor growth progression varied significantly among groups. In the Normal Saline group, tumor volume increased continuously, whereas Dox-Iodized Oil moderately suppressed tumor growth. In contrast, Dox-TIPE significantly inhibited tumor progression, with minimal volume change observed on day 14 post-embolization (Figure 3D). Quantitative analysis revealed that the average tumor volume at day 14 was 14.9 ± 6.4 cm^3 (Normal Saline), 6.7 ± 0.67 cm^3 (Dox-Iodized Oil), and 2.02 ± 1.15 cm^3 (Dox-TIPE) (Figure 3E). The tumor growth rate reached 763.7 ± 189.5% in the Normal Saline group, compared to 309.4 ± 55.8% in the Dox-Iodized Oil group and only 102.7 ± 31.2% in the Dox-TIPE group, with statistically significant differences among groups (Figure 3F; $P<0.05$ for Dox-Iodized Oil vs. Saline; $P<0.001$ for Dox-TIPE vs. Saline).

Postmortem examination on day 14 revealed extensive peritoneal and pulmonary metastases in the Normal Saline group. No peritoneal metastasis was observed in either the Dox-Iodized Oil or Dox-TIPE groups; however, pulmonary

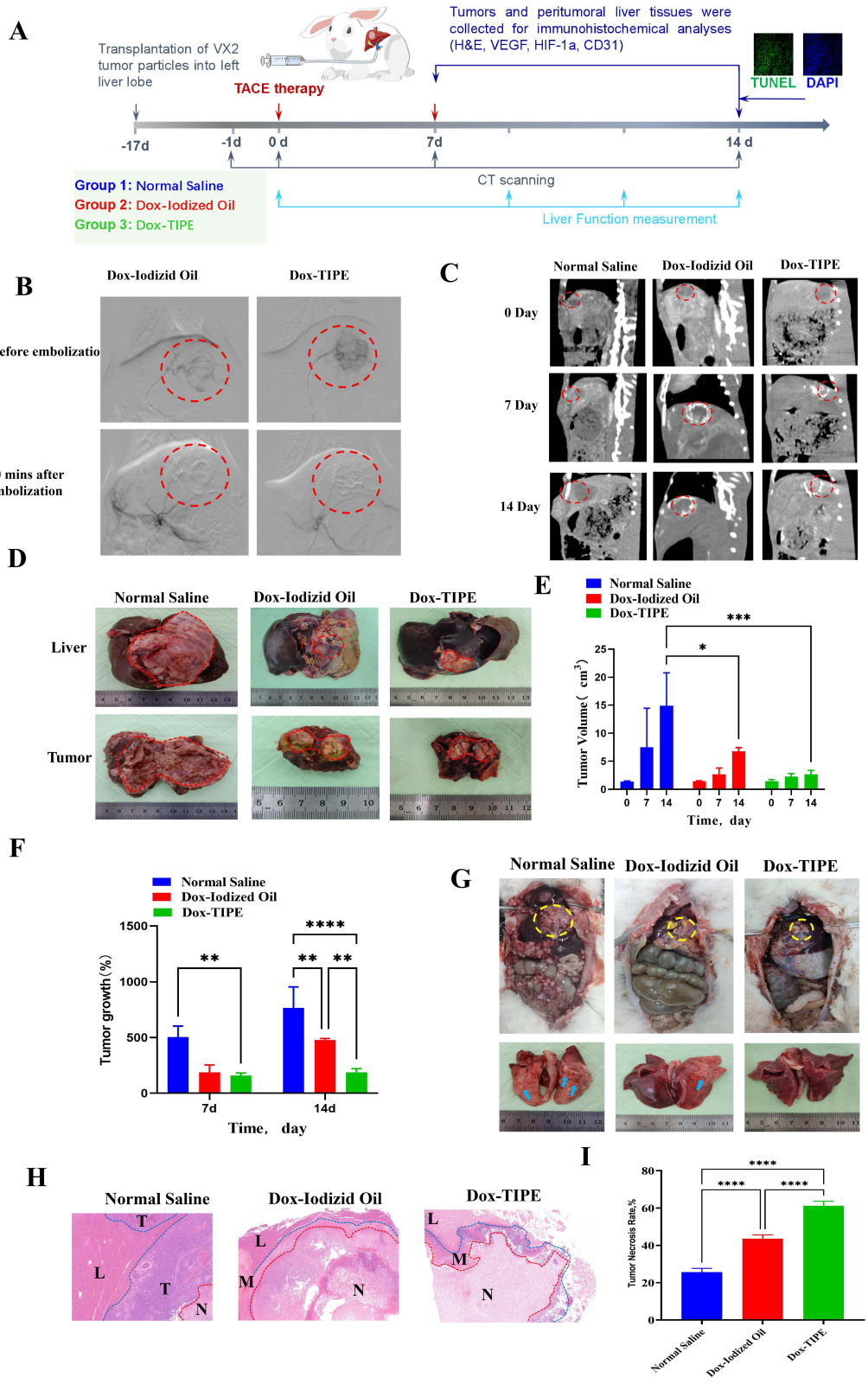

Figure 3 Intraoperative and postoperative imaging and evaluation of long-term embolization effect of Dox-TIPE. (**A**) In vivo experimental protocol of TAE and RFA. (**B**) DSA images before TACE embolization and 10 minutes after embolization, the red dotted circle marks the tumor location. The embolized tumor is indicated by the red dotted circle. (**C**) Sagittal CT images of Normal Saline, Dox-Iodized Oil, and Dox-TIPE at 0 d, 7 d, and 14d after hepatic tumor embolization. The embolized tumor is indicated by the red dotted circle. (**D**) Gross maps of tumor tissue. The embolized tumor is indicated by the red dotted circle. (**E**) Liver tumor volume. (**F**) tumor growth rate. (**G**) Abdominal and lung metastases of Normal Saline, Dox-Iodized Oil and Dox-TIPE after 14 days of liver tumor embolization. The embolized tumor is indicated by the yellow dotted circle, and the metastases is indicated by the blue arrow. (**H**) H&E staining of liver tumor tissue, T for tumor area, L for liver tissue, N for necrotic area, M for tumor boundary, scale: 2 mm. (**I**) Analysis of tumor necrosis rate. *$P < 0.05$, **$P < 0.01$, ***$P < 0.001$, ****$P < 0.0001$.

https://doi.org/10.2147/IJN.S569851

nodules were still detected in the Dox-Iodized Oil group (Figure 3G). H&E staining of tumor sections further confirmed these findings: the Normal Saline group showed multiple metastatic lesions with minimal necrosis, while both treatment groups exhibited larger areas of tumor necrosis (Figure 3H; Figure S6). Quantitative analysis revealed tumor necrosis rates of 25.6 ± 2.1% (Saline), 43.5 ± 2.1% (Dox-Iodized Oil), and 61.2 ± 2.4% (Dox-TIPE), with statistically significant differences among all groups (P<0.001) (Figure 3I).

Pharmacodynamic Evaluation of Dox-TIPE

To evaluate the intratumoral drug distribution and release kinetics, liver tumor tissues were collected from VX2 tumor-bearing rabbits on days 1, 3, and 14 post-TACE, and frozen sections were prepared for doxorubicin fluorescence imaging. Quantitative analysis of fluorescence intensity revealed a sustained release of doxorubicin in the Dox-TIPE group (Figure 4A). Unlike the Dox-Iodized Oil group, which showed a rapid release peak on day 1 followed by a steep decline, Dox-TIPE maintained drug retention in tumor tissues, with significantly higher fluorescence intensity observed from day 3 onward (P<0.001 on day 14, Figure 4B). This sustained intratumoral accumulation may reduce systemic toxicity and enhance the therapeutic window of TACE.

To further investigate treatment efficacy at the cellular level, TUNEL and Ki67 immunofluorescence staining were performed to assess tumor cell apoptosis and proliferation, respectively. TUNEL staining showed the strongest green fluorescence in the Dox-TIPE group, indicating the highest level of apoptosis among all groups (Figure 4C). Quantitative analysis demonstrated apoptosis rates of 1.8 ± 0.9% (Normal Saline), 40.6 ± 8.2% (Dox-Iodized Oil), and 64.4 ± 6.5% (Dox-TIPE) after 14 days of treatment (Figure 4D). Apoptotic activity was particularly elevated at the tumor–normal tissue interface, accompanied by reduced cell proliferation.

Ki67 staining showed a marked reduction in red fluorescence in the Dox-TIPE group compared to the other groups (Figure 4E). Tumor cell proliferation rates were 82.1 ± 9.6% in the Normal Saline group, 58.4 ± 4.8% in the Dox-Iodized Oil group, and only 27.8 ± 7.9% in the Dox-TIPE group, with statistically significant differences among groups (Figure 4F, P<0.001).

In summary, Dox-TIPE effectively achieved durable embolization of tumor vasculature and sustained intratumoral doxorubicin release, leading to enhanced apoptosis and suppressed proliferation of tumor cells. These findings suggest a synergistic benefit of combining embolization and localized chemotherapy in TACE treatment.

Effects of Dox-TIPE on Hypoxic Immune Microenvironment After Embolization of VX2 Liver Tumors

Tumor angiogenesis, a critical hallmark of hepatocellular carcinoma (HCC) progression and metastasis, sustains rapid tumor growth and facilitates systemic dissemination.[30–32] Transcatheter arterial chemoembolization (TACE) abruptly disrupts tumor blood supply, thereby inducing profound intra-tumoral hypoxia. This hypoxic milieu serves as a potent driver of compensatory neovascularization and metabolic reprogramming—two tightly coupled processes that underlie post-TACE tumor recurrence and therapeutic resistance.[33–35] Central to this adaptive response is hypoxia-inducible factor-1α (HIF-1α), the master transcriptional regulator that orchestrates the expression of key effector molecules. HIF-1α upregulates vascular endothelial growth factor (VEGF) to stimulate collateral vessel formation and concurrently enhances glucose transporter 1 (GLUT1) expression to shift tumor metabolism toward aerobic glycolysis.[36,37] Notably, VEGF is preferentially overexpressed in residual viable tumor cells at the necrotic margins following TACE, where it promotes endothelial repair, angiogenesis, and increased vascular permeability, ultimately restoring tumor perfusion.

Our findings demonstrate that Dox-TIPE exerts a dual inhibitory effect on both hypoxia-driven angiogenesis and metabolic adaptation. Quantitative fluorescence analysis revealed that Dox-TIPE treatment significantly attenuated HIF-1α expression compared to the Dox-Iodized Oil control (Figure 5A and B), suggesting a superior embolic effect that mitigates hypoxic stress within the tumor. In parallel, Dox-TIPE potently suppressed VEGF expression (Figure 5A and C), directly inhibiting the pro-angiogenic signaling cascade responsible for collateral vessel development. Importantly, we also observed a pronounced downregulation of GLUT1 in the Dox-TIPE group (Figure 5A and D). As a pivotal mediator of the Warburg effect, GLUT1 facilitates glucose uptake, enabling tumor cell survival and proliferation under nutrient-

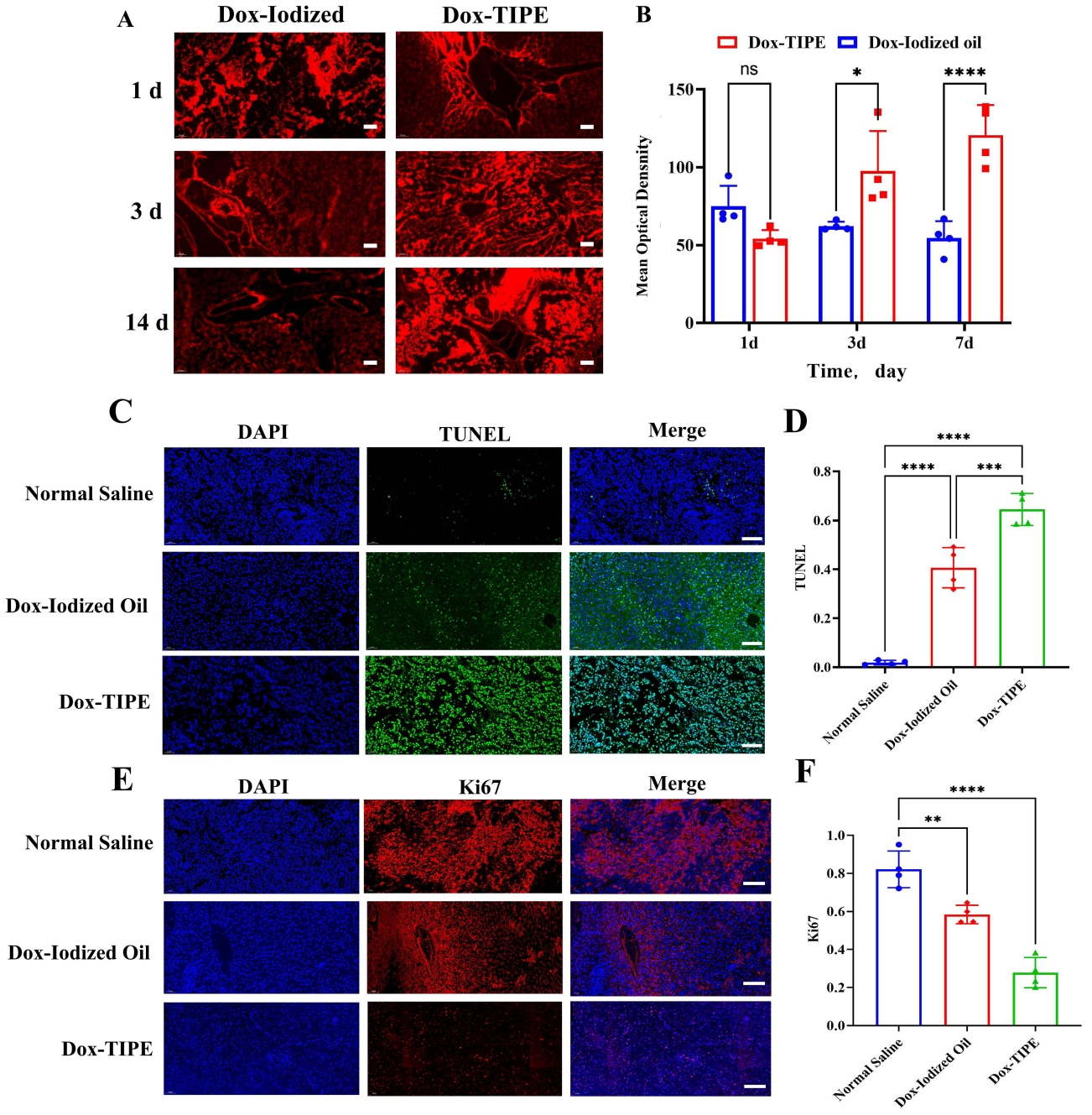

Figure 4 Pharmacodynamic evaluation of Dox-TIPE. (**A**) Dox-Iodized Oil and Dox-TIPE fluorescence pictures of doxorubicin in liver tumor tissue 1d, 3 d, and 14 d after hepatic artery embolization, magnification ×50, scale bar: 200 μm. (**B**) Fluorescent quantitative analysis of doxorubicin in liver tumor tissues at different time periods. (**C**) Immunofluorescence images of DAPI and TUNEL (magnification ×200), scale bar: 100μm. DAPI is the blue staining of the nuclei of living cells in the tissue, and the bright green fluorescence of TUNEL staining is the hallmark of tumor cell apoptosis. (**D**) Comparison of TUNEL proliferation rate. (**E**) Immunofluorescence images of DAPI and Ki67 (magnification ×200), scale bar: 100μm. DAPI is the blue staining of the nuclei of living cells in the tissue, and the bright red fluorescence of Ki67 staining is a marker of tumor cell proliferation. (**F**) Comparison of apoptosis rate of Ki67. ns: $P \geq 0.05$, *$P < 0.05$, **$P < 0.01$, ***$P < 0.001$, ****$P < 0.0001$.

deprived, hypoxic conditions.[37,38] By concurrently inhibiting GLUT1, Dox-TIPE disrupts the metabolic rewiring essential for residual tumor cell persistence, thereby complementing its anti-angiogenic action to eradicate viable tumor foci and reduce recurrence risk. This coordinated targeting of both vascular supply and energy metabolism addresses a key limitation of conventional TACE, in which residual hypoxic cells often evade treatment and drive disease progression.

To further corroborate the anti-angiogenic potency of Dox-TIPE, we evaluated CD31 expression, a well-established marker of endothelial cells and neovascularization. At 14 days post-embolization, the Dox-Iodized Oil group showed only

https://doi.org/10.2147/IJN.S569851

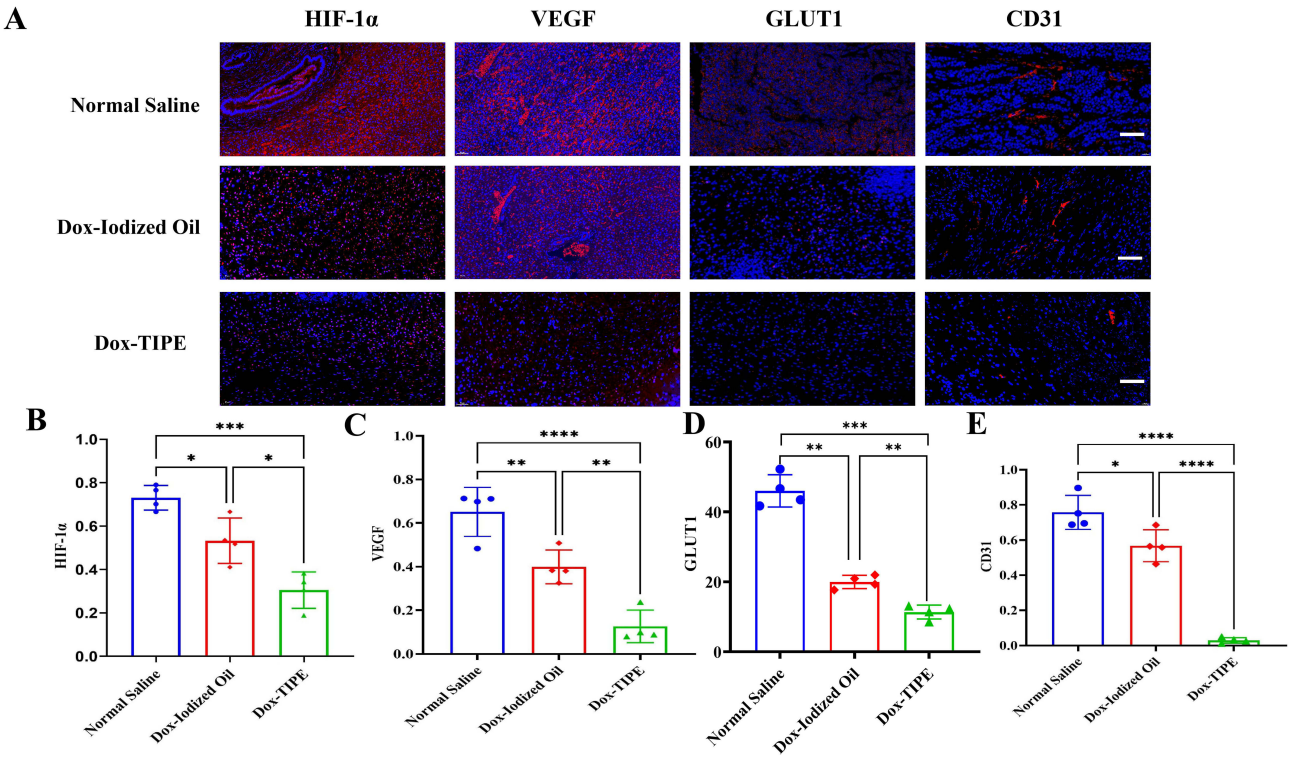

Figure 5 Immunofluorescence evaluation of the expression of HIF-lα, VEGF, GLUT1 and CD31. (**A**) Immunofluorescence images of DAPI and HIF-lα, VEGF, GLUT1 and CD31. (magnification: ×200); scale bar: 100 μm. DAPI stained the nuclei of living cells blue, and bright red fluorescence was found for HIF-lα, VEGF, GLUT1 and CD31. (**B**) Quantitative comparison of the fluorescence intensity of HIF-1α. (**C**) Quantitative comparison of the fluorescence intensity of VEGF. (**D**) Quantitative comparison of the fluorescence intensity of GLUT1. (**E**) Quantitative comparison of CD31 fluorescence intensity. *$P < 0.05$, **$P < 0.01$, ***$P < 0.001$, ****$P < 0.0001$.

a partial reduction in CD31 fluorescence intensity relative to the Normal Saline group ($P < 0.05$), indicating incomplete suppression of angiogenesis and collateral formation. In contrast, CD31 levels in the Dox-TIPE group were significantly lower than those in both control groups ($P < 0.001$; Figure 5A and E), confirming that Dox-TIPE achieves a more complete and sustained embolic effect, effectively inhibiting tumor vascular remodeling and recanalization. Collectively, these results illustrate that Dox-TIPE exerts multimodal antitumor activity by simultaneously targeting three pivotal mechanisms of post-TACE recurrence: hypoxia-driven angiogenesis, metabolic reprogramming, and vascular regeneration.

The Improvement on Post-Operative Tumor Microenvironment

To evaluate the immunomodulatory impact of Dox-TIPE after tumor embolization, we quantitatively analyzed the infiltration of $CD3^+$, $CD4^+$, and $CD8^+$ T lymphocytes in VX2 liver tumor tissues using immunofluorescence staining.[38,39] The results revealed that $CD3^+$, $CD4^+$ cells and $CD8^+$ T cells were increased in number in the tumor sections derived from rabbits treated with Dox-TIPE group and Dox-Iodized Oil group compared to those treated with NS post-TACE (Figure 6A–D). Quantitative analysis confirmed these findings: compared to the Normal Saline group, Dox-TIPE treatment significantly increased $CD3^+$ T-cell density by approximately 70% ($P < 0.001$), $CD4^+$ T-cell infiltration by about 3-fold ($P < 0.001$), and $CD8^+$ T-cell density by roughly 2.5-fold (**$P < 0.001$). Moreover, Dox-TIPE also demonstrated superior enhancement of T-cell infiltration relative to the Dox-Iodized Oil group, with increases of approximately 40% for $CD3^+$ (*$P < 0.01$), 2-fold for $CD4^+$ (*$P < 0.01$), and 1.5-fold for $CD8^+$ T cells (*$P < 0.01$). These results indicate that Dox-TIPE not only achieves effective vascular occlusion but also actively reshapes the tumor immune microenvironment (TIME) by robustly promoting T-cell infiltration, with a notable emphasis on cytotoxic $CD8^+$ T lymphocytes.

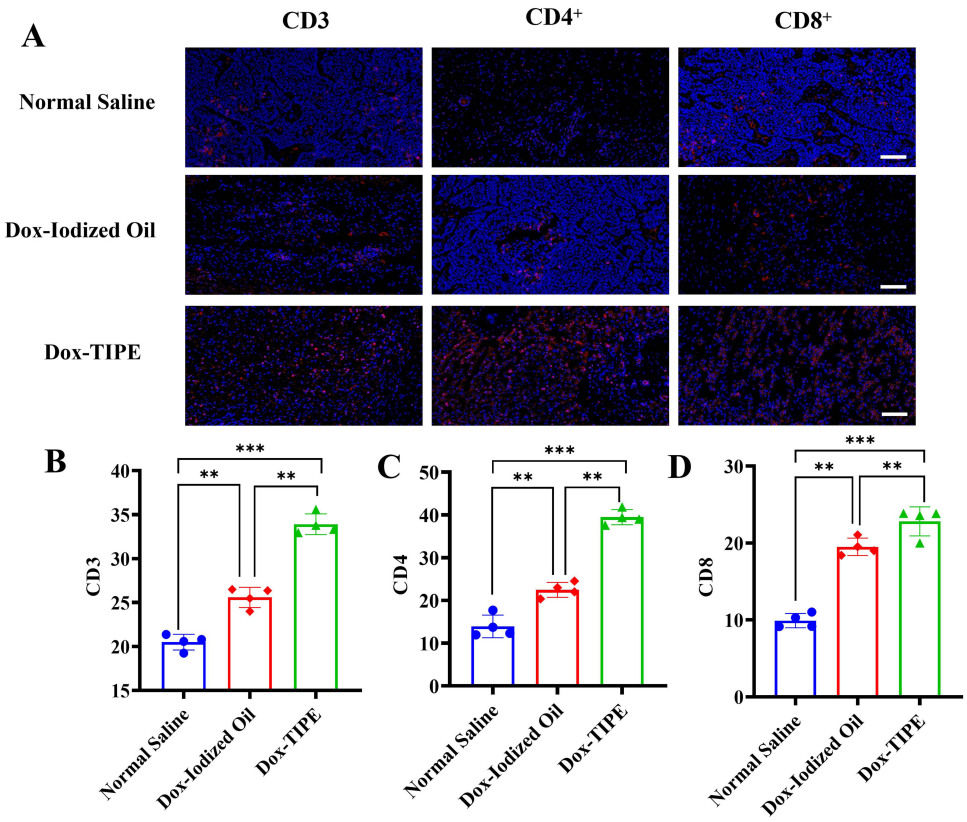

Figure 6 Immunofluorescence evaluation of CD3, $CD4^+$ and $CD8^+$. (**A**) Immunohistochemical staining of CD3, $CD4^+$ and $CD8^+$. The scale bar: 100 μm. (**B**–**D**) Quantitative comparison of CD3, $CD4^+$ and $CD8^+$. $^{**}P<0.01$, $^{***}P < 0.001$.

Biocompatibility

The biocompatibility of embolic materials is a key prerequisite for their in vivo application. In this study, PNCAA, Iodized Oil, and TIPE were diluted to concentrations ranging from 6.25 to 100 μg/mL and incubated with a 2% suspension of normal rabbit red blood cells. Normal saline and ultrapure water were used as negative and positive controls, respectively. As expected, ultrapure water induced significant hemolysis, whereas PNCAA, Iodized Oil, and TIPE showed hemolysis rates below 5%, similar to the saline control, indicating good hemocompatibility (Figure 7A).

To assess cytotoxicity, Iodized Oil and TIPE were further diluted to concentrations of 12.5, 62.5, 125, 250, and 500 μg/mL and co-incubated with HepG2 liver cancer cells for 24 h, showing high cell viability across all doses. When the concentration of TIPE was fixed and the doxorubicin in Dox-TIPE was varied (0.5–20 μg/mL), a dose-dependent decrease in cell viability was observed. The survival rates of HepG2 cells treated with Dox-TIPE were 59.7 ± 2.4%, 46.8 ± 4.5%, 41.4 ± 4.2%, 25.1 ± 4.0%, and 14.1 ± 1.7%, respectively (Figure 7B), comparable to those of the free Dox group: 61.7 ± 9.1%, 53.9 ± 2.6%, 28.8 ± 5.6%, 27.6 ± 4.3%, and 13.8 ± 2.3% (Figure 7C). These results confirm that Dox-TIPE retains the cytotoxicity of free Dox and can effectively inhibit the proliferation of HepG2 cells. A similar trend/results were also observed in normal hepatocellular cells (Figure S7).

Body weight changes in rabbits were recorded on days 0, 3, 7, and 14 post-TACE, and relative body weight indices were calculated. On day 3, all groups exhibited weight loss due to postoperative stress and decreased appetite. By day 7, rabbits in the Dox-TIPE group showed recovery in body weight and feeding behavior, whereas those in the Normal Saline and Dox-Iodized Oil groups continued to lose weight, with poor mental state and dull fur, indicating progressive tumor burden. By day 14, the differences in relative body weight among groups were statistically significant (Figure 7D). On day 14, major organs (heart, kidney, lung, spleen and normal liver) were harvested for histological examination. H&E staining revealed no obvious pathological changes in these organs across all groups, suggesting that doxorubicin delivered via Dox-TIPE did not cause systemic toxicity to major organs (Figure 7E). To investigate the cytotoxic

https://doi.org/10.2147/IJN.S569851

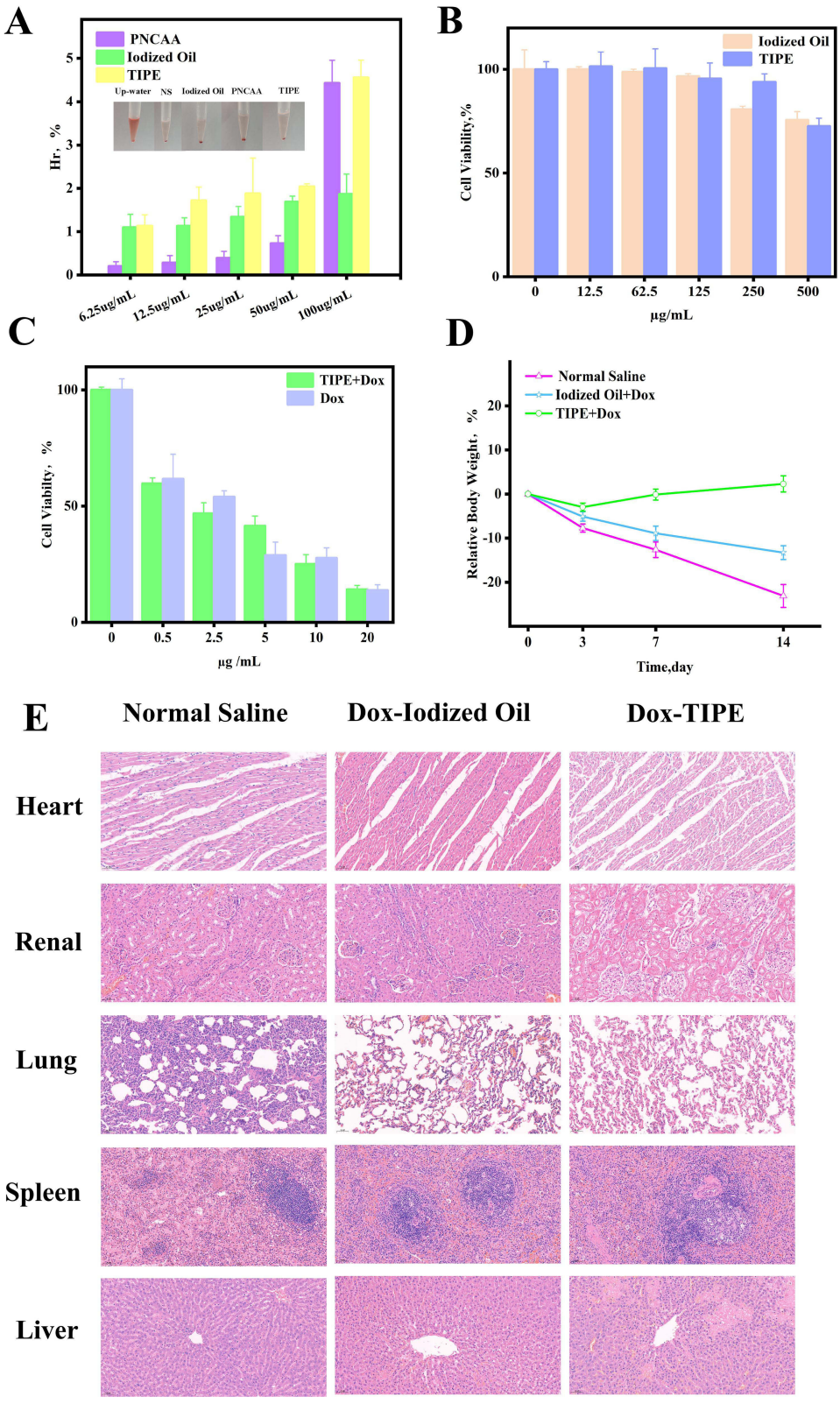

Figure 7 Biocompatibility evaluation of DOX-TIPE. (**A**) Analysis of the rabbit hemolysis rate. (**B**) Iodized oil and TIPE were incubated with HepG2 liver cancer cells at different concentrations. Survival rate after 24 h. (**C**) Dox and Dox-TIPE were incubated with HepG2 liver cancer cells at different concentrations, and the survival rates were determined after 24 h. (**D**) H&E staining of heart, kidney, lung, spleen, and normal liver tissues. (**E**) The relative body mass index of rabbits.

https://doi.org/10.2147/IJN.S569851

mechanism, HepG2 cells treated with Dox-TIPE, DOX, TIPE, or saline were subjected to Annexin V-FITC/PI staining and flow cytometric analysis. The results indicate that DOX acts as a potent cytotoxic agent, inducing substantial cell necrosis and apoptosis. In contrast, TIPE alone exhibits only a modest pro-apoptotic effect and demonstrates neither synergistic nor antagonistic activity when co-administered with DOX (Figure S8 and S9).

Conclusion

In this study, we developed a novel oil-in-water (O/W) Pickering emulsion hydrogel composite known as Dox-TIPE, which integrates thermosensitivity, radiopacity, and drug delivery functionality. In vitro drug release experiments demonstrated that under slightly acidic conditions (pH 6.8), 20Dox-TIPE exhibits a sustained-release profile well-suited for localized chemotherapy in the tumor microenvironment. In vivo embolization studies using a VX2 liver tumor-bearing rabbit model showed Dox-TIPE achieved the most effective therapeutic outcome, providing superior hepatic artery embolization and sustained drug release that synergistically inhibited tumor progression. Further immunohistochemical analyses demonstrated that the formulation significantly improved the tumor immune microenvironment, induced tumor cell necrosis and apoptosis, and facilitated the sustained release of doxorubicin, resulting in a synergistic chemoembolization effect.

DOX-TIPE exhibits excellent rheological properties, enabling it to reach distal tumor vasculature efficiently. Upon entering the bloodstream, it rapidly responds to physiological temperature and undergoes in situ solidification within tumor vessels upon reaching its phase-transition temperature. Given the weakly acidic tumor microenvironment, drug release kinetics studies confirmed that DOX-TIPE achieves maximal drug release under weakly acidic conditions. This suggests that DOX-TIPE can also maintain favorable release performance in the acidic microenvironment of tumor vasculature. Consistent with these findings, animal experiments demonstrated that DOX-TIPE yields the optimal therapeutic outcome. In conclusion, Dox-TIPE offers a multifunctional platform combining embolization, chemotherapy, imaging, and immunomodulation. This novel embolic material shows strong potential to address current limitations of TACE in liver cancer treatment and may serve as a promising candidate for next-generation embolization therapies.

Funding

This work was supported by Hubei Province Nature Science Foundationof China (2025AFB917), Doctoral Start-up Fund Project of Hubei University of Science and Technology (BK202118, BK202335), Innovation team and Medical research program of Hubei University of Science and Technology (2023T10, 2022YKY05), Horizontal Project of Hubei University of Science and Technology (2025HX121, 2025HX148, 2024HX161, 2025HX167, 2025HX160), Hubei Provincial Key Laboratory for Operation and Control of Cascaded Hydropower StationFund Project (2023KJX02), Guiding Project of Scientific Research Plan of Hubei Provincial Department of Education in 2024 (B2024159).

Disclosure

The authors declare that they have no competing interests.

References

1. Vogel A, Meyer T, Sapisochin G, et al. Hepatocellular carcinoma. *Lancet*. 2022;400(10360):1345–1362. doi:10.1016/S0140-6736(22)01200-4
2. Hartke J, Johnson M, Ghabril M. The diagnosis and treatment of hepatocellular carcinoma. *Seminars Diagnostic Pathol*. 2017;34(2):153–159. doi:10.1053/j.semdp.2016.12.011
3. Gong F, Zheng LY, Xu JH, et al. Magnesium microspheres for enhanced transarterial chemoembolization therapy of hepatocellular carcinoma: from animal models to a pilot clinical study. *Sci Adv*. 2025;11(27):eadv0885. doi:10.1126/sciadv.adv0885
4. Duan XH, Li H, Kuang DL, et al. Comparison of drug-eluting bead transarterial chemoembolization combined with apatinib versus drug-eluting bead transarterial chemoembolization for the treatment of unresectable hepatocellular carcinoma: a randomized, prospective, multicenter Phase III trial. *Signal Transduction Targeted Therapy*. 2024;9(1):304. doi:10.1038/s41392-024-02012-x
5. Liang J, Bai Y, Ha F-S, et al. Combining local regional therapy and systemic therapy: expected changes in the treatment landscape of recurrent hepatocellular carcinoma. *World J Gastrointest Oncol*. 2023;15(1):1–18. doi:10.4251/wjgo.v15.i1.1
6. Chen MJ, Lu QW, Gong F, et al. A gas nanobomb to promote drug penetration and amplify TACE therapy for orthotopic liver tumor. *Adv Mater*. 2025;37(39):e2505770. doi:10.1002/adma.202505770
7. Sutanto H, Adytia GJ, Elisa E, et al. Advances in transarterial chemoembolization for hepatocellular carcinoma: integration with systemic therapies and emerging treatment strategies. *Mater Today Bio*. 2025;3:E01–E13.

8. Miyayama S. Ultraselective conventional transarterial chemoembolization: when and how? *Clin Mole Hepatol*. 2019;25(4):344–353. doi:10.3350/cmh.2019.0016
9. Li Z, Di C, Li S, et al. Smart nanotherapeutic targeting of tumor vasculature. *Acc Chem Res*. 2019;52(9):2703–2712. doi:10.1021/acs.accounts.9b00283
10. Fuchs AK, Duran BR, Denys BA, et al. Drug-eluting embolic microspheres for local drug delivery – state of the art. *J Control Release*. 2017;262:127–138. doi:10.1016/j.jconrel.2017.07.016
11. Raoul J-L, Sangro B, Forner A, et al. Evolving strategies for the management of intermediate-stage hepatocellular carcinoma: available evidence and expert opinion on the use of transarterial chemoembolization. *Cancer Treat Rev*. 2011;37(3):212–220. doi:10.1016/j.ctrv.2010.07.006
12. Raoul J-L, Forner A, Bolondi L, et al. Updated use of TACE for hepatocellular carcinoma treatment: how and when to use it based on clinical evidence. *Cancer Treat Rev*. 2019;72:28–36. doi:10.1016/j.ctrv.2018.11.002
13. Tam KY, Leung KC-F, Wang Y-XJ. Chemoembolization agents for cancer treatment. *Eur J Pharm Sci*. 2011;44(1–2):1–10. doi:10.1016/j.ejps.2011.06.013
14. Shin SW. The current practice of transarterial chemoembolization for the treatment of hepatocellular carcinoma. *Korean Radiol*. 2009;10(5):425–434. doi:10.3348/kjr.2009.10.5.425
15. Ebeling Barbier C, Heindryckx F, Lennernäs H. Limitations and possibilities of transarterial chemotherapeutic treatment of hepatocellular carcinoma. *Int J Mol Sci*. 2021;22(23):13051. doi:10.3390/ijms222313051
16. Yao L, Wang Y, He Y, et al. Pickering emulsions stabilized by conjugated zein-soybean polysaccharides nanoparticles: fabrication, characterization and functional performance. *Polymers*. 2023;15(23):4474. doi:10.3390/polym15234474
17. Li Z, Xu W, Yang J, et al. A tumor microenvironments-adapted polypeptide hydrogel/nanogel composite boosts antitumor molecularly targeted inhibition and immunoactivation. *Adv Mater*. 2022;34(21):e2200449. doi:10.1002/adma.202200449
18. Zhao Y, Zhang Z, Pan Z, et al. Advanced bioactive nanomaterials for biomedical applications. *Exploration*. 2021;1(3):20210089. doi:10.1002/EXP.20210089
19. Wu J, Ma G. Recent studies of pickering emulsions: particles make the difference. *Small*. 2016;12:4633e4648.
20. McClements DJ, Gumus CE. Natural emulsifiers — biosurfactants, phospholipids, biopolymers, and colloidal particles: molecular and physicochemical basis of functional performance. *Adv Colloid Interface Sci*. 2016;234:3e26. doi:10.1016/j.cis.2016.03.002
21. Chen H, Zhu H, Hu J, et al. Highly compressed assembly of deformable nanogels into nanoscale suprastructures and their application in nanomedicine. *ACS Nano*. 2011;5(4):2671e2680. doi:10.1021/nn102888c
22. Xie W, Li H, Yu H, et al. A thermosensitive pickering gel emulsion with a high oil–water ratio for long-term X-ray imaging and permanent embolization of arteries. *Nanoscale*. 2023;15(4):1835–1848. doi:10.1039/D2NR05963K
23. Li L, Guo A, Sun H, et al. Research and application of thermosensitive pickering emulsion with X-ray and ultrasound dual-modal imaging functions for intra-arterial embolization treatment. *J Pharm Anal*. 2025;15(4):101133. doi:10.1016/j.jpha.2024.101133
24. Zhou HF, Xie WJ, Guo AR, et al. Temperature sensitive nanogels for real-time imaging during transcatheter arterial embolization. *Designed Monomers Polymers*. 2023;26(1):31–44. doi:10.1080/15685551.2022.2164445
25. Li H, Qian K, Zhang H, et al. Pickering gel emulsion of lipiodol stabilized by hairy nanogels for intra-artery embolization antitumor therapy. *Chem Eng J*. 2021;418:129534. doi:10.1016/j.cej.2021.129534
26. Kong C-Y, Guo Z, Song P, et al. Underlying the mechanisms of doxorubicin-induced acute cardiotoxicity: oxidative stress and cell death. *Int J Bio Sci*. 2022;18(2):760–770. doi:10.7150/ijbs.65258
27. Wu BB, Leung KT, Poon EN-Y. Mitochondrial-targeted therapy for doxorubicin-induced cardiotoxicity. *Int J Mol Sci*. 2022;23(3):1912. doi:10.3390/ijms23031912
28. Choi YC, Jung K. Normalization of the tumor microenvironment by harnessing vascular and immune modulation to achieve enhanced cancer therapy. *Exp Mol Med*. 2023;55(11):2308–2319. doi:10.1038/s12276-023-01114-w
29. Sun XW, Wang D, Chang SW, et al. Development of cytolytic iridium-complexed octaarginine peptide albumin nanomedicine for hepatocellular carcinoma treatment. *Int J Nanomedicine*. 2025;25:2395–2409.
30. Couri T, Pillai A. Goals and targets for personalized therapy for HCC. *Hepatol Internat*. 2019;13(2):125–137. doi:10.1007/s12072-018-9919-1
31. Viallard C, Larrivée B. Tumor angiogenesis and vascular normalization: alternative therapeutic targets. *Angiogenesis*. 2017;20(4):409–426. doi:10.1007/s10456-017-9562-9
32. Lugano R, Ramachandran M, Dimberg A. Tumor angiogenesis: causes, consequences, challenges and opportunities. *Cellular Mole Life Sci*. 2020;77(9):1745–1770. doi:10.1007/s00018-019-03351-7
33. Masoud GN, Li W. HIF-1α pathway: role, regulation and intervention for cancer therapy. *Acta Pharmaceutica Sinica B*. 2015;5(5):378–389. doi:10.1016/j.apsb.2015.05.007
34. Siveen KS, Prabhu K, Krishnankutty R, et al. Vascular Endothelial Growth Factor (VEGF) signaling in tumour vascularization: potential and challenges. *Curr Vasc Pharmacol*. 2017;15(4):339–351. doi:10.2174/1570161115666170105124038
35. Zhao Y, Adjei AA. Targeting angiogenesis in cancer therapy: moving beyond vascular endothelial growth factor. *oncologist*. 2015;20(6):660–673. doi:10.1634/theoncologist.2014-0465
36. Jiang X, Wang J, Deng X, et al. The role of microenvironment in tumor angiogenesis. *J Exp Clin Cancer Res*. 2020;39(1):204. doi:10.1186/s13046-020-01709-5
37. Teleanu RI, Chircov C, Grumezescu AM, et al. Tumor angiogenesis and anti-angiogenic strategies for cancer treatment. *J Clin Med*. 2019;9(1):84. doi:10.3390/jcm9010084
38. Zhang Q, Shi D, Guo M, et al. Radiofrequency-activated pyroptosis of bi-valent gold nanocluster for cancer immunotherapy. *ACS Nano*. 2023;17(1):515–529. doi:10.1021/acsnano.2c09242
39. Yu J, Fu Y, Gao J, et al. Cathepsin C from extracellular histone-induced M1 alveolar macrophages promotes NETosis during lung ischemia-reperfusion injury. *Redox Biol*. 2024;74:103231. doi:10.1016/j.redox.2024.103231